Nuclear Materials and Energy 33 (2022) 101294

Contents lists available at ScienceDirect

Nuclear Materials and Energy

journal homepage: www.elsevier.com/locate/nme

Three-dimensional structure of radiative cooling in impurity seeded plasmas in the Large Helical Device

K. Mukai [a,b,*], G. Kawamura [a,b], S. Masuzaki [a,b], Y. Hayashi [a,b], H. Tanaka [c], B.J. Peterson [a,b], T. Oishi [a,b], C. Suzuki [a,b], M. Kobayashi [a,b], K. Munechika [d]

[a] National Institute for Fusion Science, National Institutes of Natural Sciences, Toki, Japan
[b] The Graduate University for Advanced Studies, SOKENDAI, Toki, Japan
[c] Institute of Materials and Systems for Sustainability, Nagoya University, Nagoya, Japan
[d] Tokyo Institute of Technology, Tokyo, Japan

ARTICLE INFO

Keywords:
IRVB
Imaging bolometer
PCA
Detachment
EMC3-EIRENE
LHD

ABSTRACT

Three-dimensionally localization of radiative cooling due to nitrogen (N_2) seeding for divertor detachment was detected experimentally. Since the localization along some magnetic field lines induces toroidal asymmetry of heat load reduction on divertor plates, it should be avoided for fusion reactors. The three-dimensionally localized structure was extracted using Principal Component Analysis (PCA) from two-dimensional radiation images measured with an InfraRed imaging Video Bolometer (IRVB). By applying PCA to 34 images each in N_2 seeded plasmas with toroidally-asymmetric heat load reduction and in neon (Ne) seeded plasmas with toroidally-symmetric heat load reduction, a radiation feature in N_2 seeded plasmas was found as one of the principal components (PC). The three-dimensional transport code EMC3-EIRENE indicated that the ionization in one of the divertor legs is enhanced in nitrogen seeding compared with Ne seeding due to the difference in the first ionization energy. The magnetic field lines from the divertor leg were along the extracted radiation structure and were terminated by the divertor where the heat load decreased due to the N_2 seeding. These results indicate that three-dimensionally localized structure of radiative cooling was detected experimentally.

Introduction

To realize fusion reactors, symmetries of torus plasmas are broken by external factors, e.g., impurity seeding for divertor detachment, resonant magnetic perturbation for suppression of edge localized modes, limiter for plasma start-up, and so on. They induce three-dimensional effects on torus plasma. For example, toroidally asymmetric behavior of divertor heat load reduction was observed in not only helical device but also tokamak device. In Alcator C-Mod, using five toroidally spaced gas injectors and toroidally fixed diagnostics, toroidal asymmetries of radiated power and nitrogen line emission were observed [1]. EMC3-EIRENE qualitatively reproduced the asymmetries and predicted a toroidal asymmetry in the heat flux to the outer divertor target [2]. In LHD, a toroidal asymmetric reduction of divertor heat flux was observed in N_2 seeded plasmas by the divertor Langmuir probe array measurement [3]. Toroidal asymmetry of radiated power was also measured with three toroidally spaced gas injectors and toroidally fixed resistive bolometer [4]. EMC3-EIRENE with the assumption of no recycling of nitrogen particles indicated the similar asymmetric characteristics of divertor heat flux reduction with the experiment around the N_2 seeding port [5]. Since the asymmetric pattern was strongly related to the magnetic field structure around the seeding port, localization of radiative cooling along magnetic field lines was implied. On the other hand, such toroidal asymmetry was not observed with both N_2 and Ne seeding in the island divertor at W7-X [6].

This toroidal asymmetry should be investigated from the viewpoint of integration of the divertor detachment and improved core confinement. In ASDEX-Upgrade, stable completely detached H-mode plasma in the full tungsten was achieved using N_2 seeding [7]. However, in DIII-D and JET-ILW, while high-performance core plasmas were integrated with fully detached divertor using N_2 seeding, they were integrated with partially detached divertor using Ne seeding [8,9]. Moreover, in EAST with ITER-like tungsten divertor, even in the H-mode plasma with Ne and deuterium seeding, toroidal asymmetry of the divertor heat load reduction was observed [10]. A simple solution to avoid the asymmetry is the impurity seeding from various positions. However, the number of

* Corresponding author.
E-mail address: mukai.kiyofumi@nifs.ac.jp (K. Mukai).

https://doi.org/10.1016/j.nme.2022.101294
Received 30 June 2022; Received in revised form 13 October 2022; Accepted 30 October 2022
Available online 3 November 2022

seeding ports should minimize in reactors to ensure the space for blanket. Therefore, to avoid the asymmetry with minimum seeding ports, the mechanism of the asymmetry should be investigated using measurements and reproduced using simulation codes. However, the localized radiation structure along the magnetic field lines was not measured in the previous works while the localization was implied. Therefore, the purpose of this study is to detect the 3-D localized radiation structure experimentally.

Experimental setup and analysis method

Experimental setup on LHD

The LHD is one of the largest helical devices with poloidal/toroidal period numbers of 2/10. The major radius is 3.9 m and the averaged minor radius is 0.6 m. Fig. 1 shows the experimental setup on LHD. The magnetic axis, R_{ax}, set to 3.60 m. The toroidal magnetic field was directed to counterclockwise with the strength of 2.75 T. The natural error field was cancelled using a perturbation coil system. Plasmas were generated using electron cyclotron heating and were sustained using three tangential neutral beam injections. Hydrogen gas was puffed from the lower port between the toroidal sections #3 and #4 (3.5-L). Impurity gases (N_2 or Ne) were puffed from the 5.5-L port. Total plasma radiated power, P_{rad}, was measured at the outer port of the toroidal sections #3 (3-O). Divertor heat load was measured with Langmuir probe arrays at inner port of the toroidal section #2, 4, 6, 7, 8, 9, and 10. All arrays consist of left-hand and right-hand side arrays as shown in Fig. 1 (b) of Ref. [3].

Two-dimensional radiation profile measurement

Two-dimensional radiation profile was measured with an IRVB. The IRVB consists of a pinhole camera with a thin metal foil absorber and an infrared (IR) camera [11,12]. Plasma radiation is projected onto the foil absorber through a pinhole. Two-dimensional temperature distribution generated by the plasma radiation is observed using the IR camera from the back side. The IRVB has been installed at the upper port (6.5-U) as shown in Fig. 1. The field of view is shown in Fig. 2. The numbers of channels are 26 and 20 in toroidal and radial direction, respectively. 520 channels in total are much larger than resistive bolometer arrays which are few ten channels usually.

Principal component analysis

To detect the three-dimensionally localized structure, three-dimensional tomography using some detectors is one of the methods. In the LHD, three-dimensional tomography succeeded using four IRVBs with the assumption of helical symmetry [13]. However, in this study, since it is considered that the structure of the target radiation is toroidally localized, the helical symmetry cannot be assumed. Therefore, PCA is applied to extract the features from two-dimensional images.

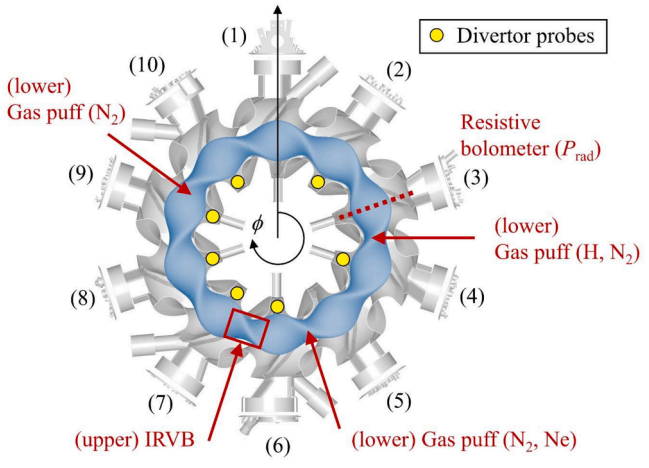

Fig. 1. Configurations of gas seeding port, bolometers, and divertor Langmuir probe arrays on the LHD.

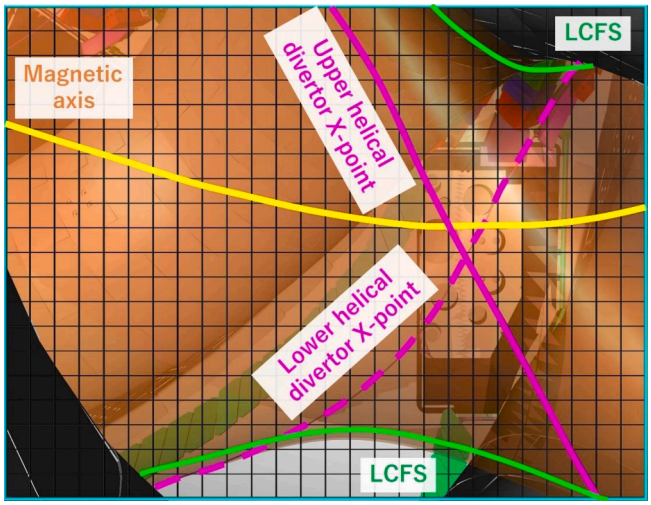

Fig. 2. Field of view of InfraRed imaging Video Bolometer (IRVB) installed at 6.5-U port.

PCA can extract the important information from the original data and describe the information as principal components (PCs) which are a set of new orthogonal variables [14,15]. PCs are calculated as linear combinations of the original variables. The first PC is evaluated to maximize the variance. The second component is evaluated under the limitation of being orthogonal to the first PC and to maximize the variance. The other PCs are calculated in the same way. The $I \times J$ matrix of original data, $\boldsymbol{X}$, can be described as $\boldsymbol{X} = \boldsymbol{F}\boldsymbol{Q}^{\mathrm{T}}$. Here, I is the total number of IRVB images. J is the total channel number of an IRVB image ($26 \times 20 = 520$). $\boldsymbol{X}$ has rank $L \leq \min\{I, J\}$. The $I \times L$ matrix, $\boldsymbol{F}$, is the set of coefficients called PC scores. The $J \times L$ matrix, $\boldsymbol{Q}$, is the set of PCs. PCA also can display the pattern of similarity of the original data and the variables as maps using PC scores. Therefore, when the distribution of a PC score is different in some experimental conditions, e.g., N_2 and Ne seeding, the PC is a feature to characterize the conditions.

Extraction of radiation feature in N_2 seeded plasmas compared with Ne seeded plasmas

Fig. 3 (a) - (f) show the typical waveforms of Ne and N_2 seeded plasmas. Ne was seeded from $t = 4.1$ s with the particle rate of 3.4 Pa·m^3/s. As shown in Fig. 3 (a) and (b), absorbed NBI power, P_{NBI}, increased after the Ne seeding since the heating efficiency improved with the increase of line-averaged electron density, $n_{e,\,bar}$. Ion saturation current measured with divertor probe arrays, $I_{sat,\,div}$, decreased after the Ne seeding with the increase of P_{rad} as shown in Fig. 3 (a) and (c). Fig. 4 (a) shows toroidal distribution of $I_{sat,\,div}$ ratio between before and after Ne seeding. Here, the timing before the seeding was defined as $t = 4.0$ s which is 0.1 s before the seeding. The timing after the seeding was determined as the timing when radiation fraction, $f_{rad} = P_{rad}/P_{NBI}$, reached the maximum. The reduction occurred in all toroidal sections (=toroidally symmetric reduction). In the case of N_2 seeding, as shown in Fig. 3 (d), N_2 was seeded from $t = 4.1$ s with the particle rate of 3.1 Pa·m^3/s. As shown in Fig. 3 (f) and Fig. 4 (b), while $I_{sat,\,div}$ decreased after the seeding in some toroidal sections, $I_{sat,\,div}$ increased in the other toroidal sections (=toroidally asymmetric reduction). Here, increase of P_{rad} after the N_2 seeding was quite small since the toroidal-localization of radiative cooling [3] should occur outside the field of view of the

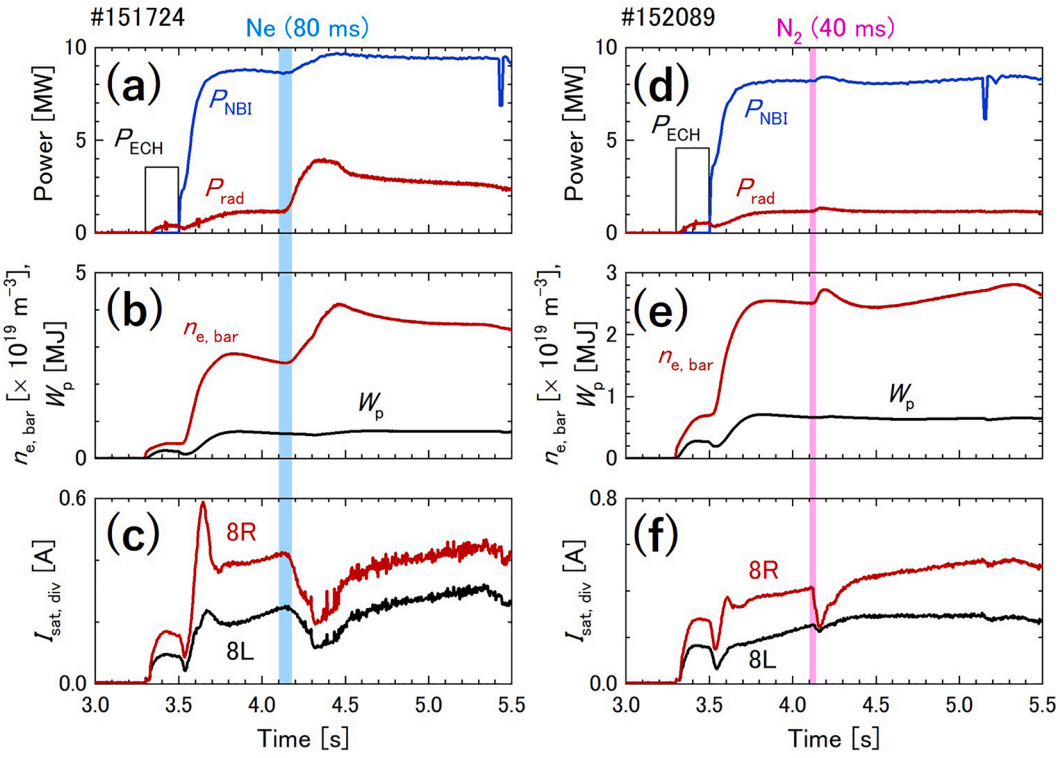

Fig. 3. Typical time evolutions of (a) heating power of ECH and NBI, P_{ECH} and P_{NBI}, with total plasma radiated power, P_{rad}, (b) line-averaged electron density, $n_{e,\,bar}$, and plasma stored energy, W_p, and (c) divertor ion saturation current, $I_{sat,\,div}$ in Ne seeded plasma. (d) - (f) Those in N_2 seeded plasma.

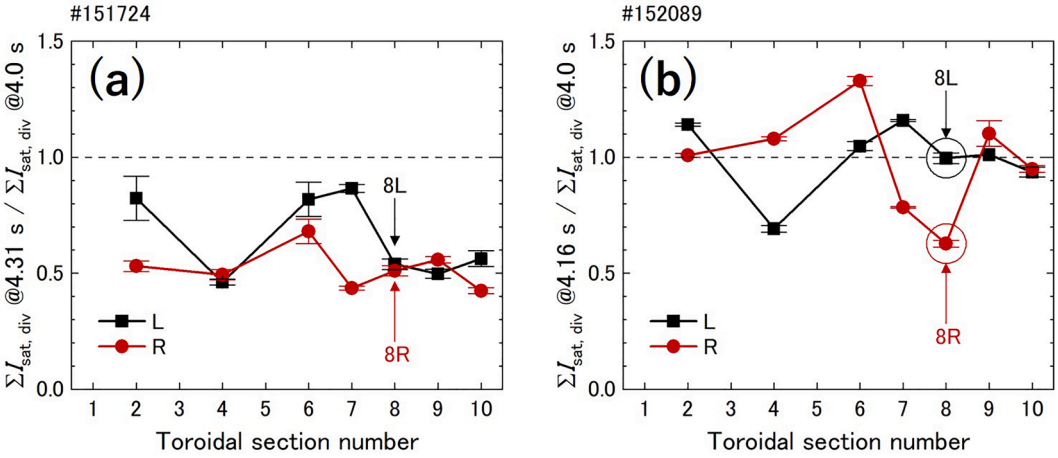

Fig. 4. Typical toroidal distribution of $I_{sat,\,div}$ ratio between before and after the (a) Ne and (b) N_2 seeded plasmas.

resistive bolometer at 3-O port as shown in Fig. 1. These asymmetries were maintained using more moderate N_2 seeding for 1 s [4].

Fig. 5 shows the typical radiation images in Ne and N_2 seeded plasmas measured with the IRVB. In order to extract the feature in the N_2 seeded plasmas, PCA was applied to the images. 34 shots of each were used for Ne and N_2 seeded plasmas. One image at the time of the maximum f_{rad} was selected in each shot. Here, $n_{e,\,bar}$ before the seeding ranged 1–5 $\times$ 10^{19} m^{-3}. Ne seeding was performed from 5.5-L port as shown in Fig. 1. N_2 seeding was performed from three different toroidal positions (8 shots from 3.5-L, 19 shots from 5.5-L, and 7 shots from 9.5-L) individually. Fig. 6 shows the first to sixth PCs of totally 68 PCs. In comparison with Fig. 2 in this paper and Fig. 10–12 in the Ref. [5], the radiation region of the PCs can be considered as follows: The first PC indicated the radiation from upper and lower helical divertor X-points (HDX) ((1) and (2) of Fig. 10–12 in the Ref. [5]). Positive and negative components of the second PC corresponded to the radiation around the upper HDX and outboard side of plasma edge region ((3) of Fig. 10–12 in the Ref. [5]), respectively. The third PC should be the radiation around the upper HDX and the outboard side. The fourth PC can be the radiation from relatively core region. The fifth or higher-order PCs did not have meaningful structures. The cumulative contribution ratio of the first PC reached 90.8 %. The quite-high ratio is caused by the low degree of freedom. Especially in helical devices, plasma confinement region is fixed by external coil currents while the targets of face or handwritten character authentication have high degree of freedom, e.g. size, shift, and rotation. Fig. 7 (a) shows the relation between the first and second PC scores. While the first PC score ranges similar in both N_2 and Ne cases from 5.5-L port, higher second PC scores were observed in N_2 cases shown in red symbols compared with those in Ne cases shown in blue symbols. It means that the positive component of the second PC shown

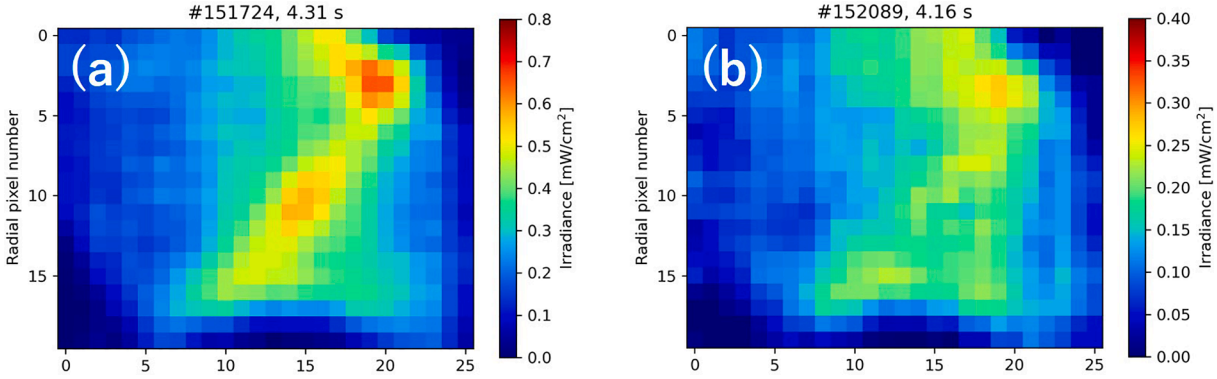

Fig. 5. Typical radiation images of IRVB in (a) Ne and (b) N_2 seeded plasmas.

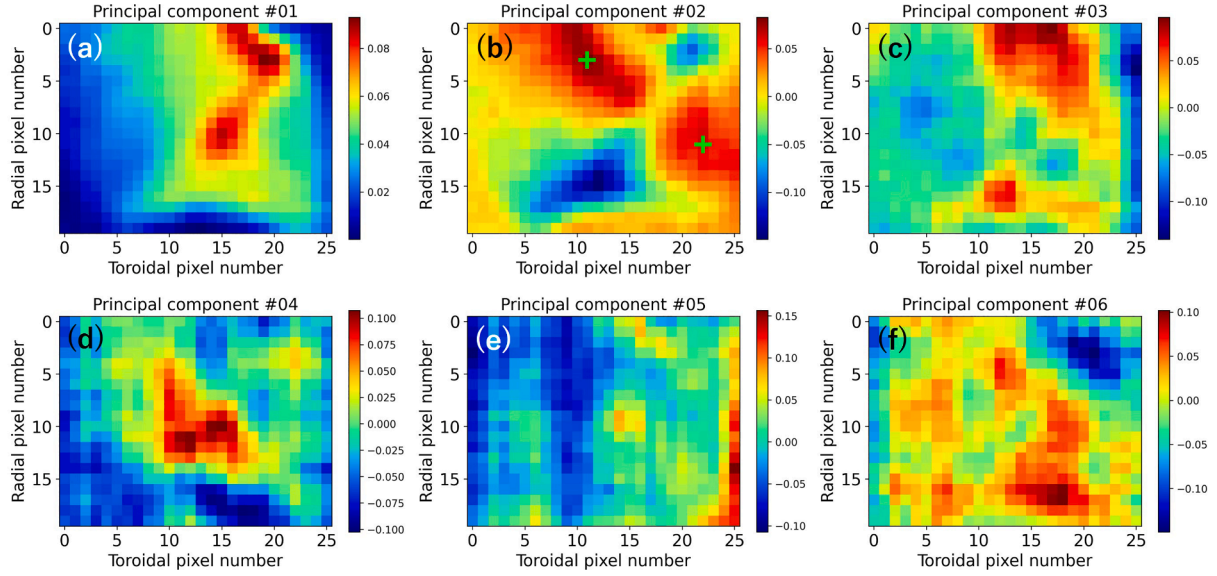

Fig. 6. (a) First to (f) sixth principal components extracted from 68 images of Ne and N_2 seeded plasmas. Cross symbols in (b) are the local maximum of the structure and eye guides for the later discussion.

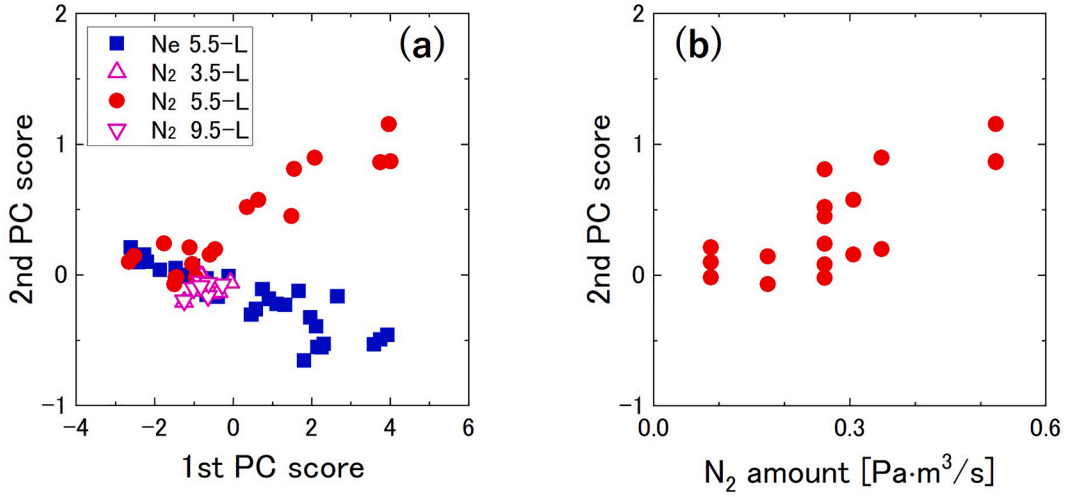

Fig. 7. (a) Relation between the first and second principal component scores. Blue and red symbols indicate Ne and N_2 seeded plasmas from 5.5-L port, respectively. Pink symbols indicate N_2 seeded plasmas from 3.5-L and 9.5-L ports. (b) The second principal component scores in the N_2 seeded plasmas from 5.5-L port as the function of the seeded amount. (For interpretation of the references to colour in this figure legend, the reader is referred to the web version of this article.)

in Fig. 6 (b) increased with the N_2 seeding from 5.5-L port. Here, the radiation images were measured with the IRVB at 6.5-U port (between the toroidal section #6 and #7) and the enhancement of the second PC score was not observed in the N_2 seeding from 3.5-L and 9.5-L ports shown in Fig. 7 (a) as pink symbols. It indicates that the radiation due to N_2 seeding was localized toroidally. The second PC score using N_2 seeding from 5.5-L port was proportional to the N_2 seeded amount as shown in Fig. 7 (b). These results indicate that the localized radiation structure due to N_2 seeding was extracted from the radiation images measured with the IRVB.

Comparison of extracted radiation structure and magnetic field line structure

To investigate the difference in the radiation structure between N_2 and Ne seeded plasmas, ionization profiles of the seeded impurities were calculated by EMC3-EIRENE with full-torus model [5,16]. Boundary conditions at the core were the heating power of 9 MW, and the electron density of 3×10^{19} m^{-3}. The transport coefficients were D = 0.5 m^2 s^{-1}, $\chi_e = \chi_i = 1.0$ m^2 s^{-1}. The impurities, Ne and nitrogen, were injected from the 5.5-L port as neutral gas with the initial speed of 0.03 eV which corresponds to the thermal speed at room temperature. Here, we should note that the injected nitrogen (N) is atomic gas because of the limitation of the code to treat molecular gas. The background plasma was assumed to be constant, i.e., the effect of ionized impurities on the ionization was not included in the calculation. Fig. 8 (a) and (b) show the calculated ionization profiles in N and Ne, respectively, at the poloidal cross section of the 5.5-L port. Fig. 8 (c) and (d) show the enlarged view of Fig. 8 (a) and (b). Since impurities were seeded from the lower port, the ionization position was distributed on the lower side of the poloidal cross section in both cases. Moreover, the ionization rate in the lower-left leg was less than that in the lower-right leg. It could be occurred by the lower electron temperature, T_e, and density, n_e, in the lower-left leg compared with those in the lower-right leg as shown in Fig. 8 (e) and (f). The lower T_e and n_e in the lower-left leg were due to the shorter connection length compared with the lower-right leg which is the characteristic of the magnetic configuration of $R_{ax} = 3.6$ m. The main difference between N and Ne was that the ionization in the lower-left divertor leg enhanced in the N seeding case compared with the Ne seeding case. N has lower first ionization energy of 14.53 eV compared with Ne of 21.56 eV. While T_e in

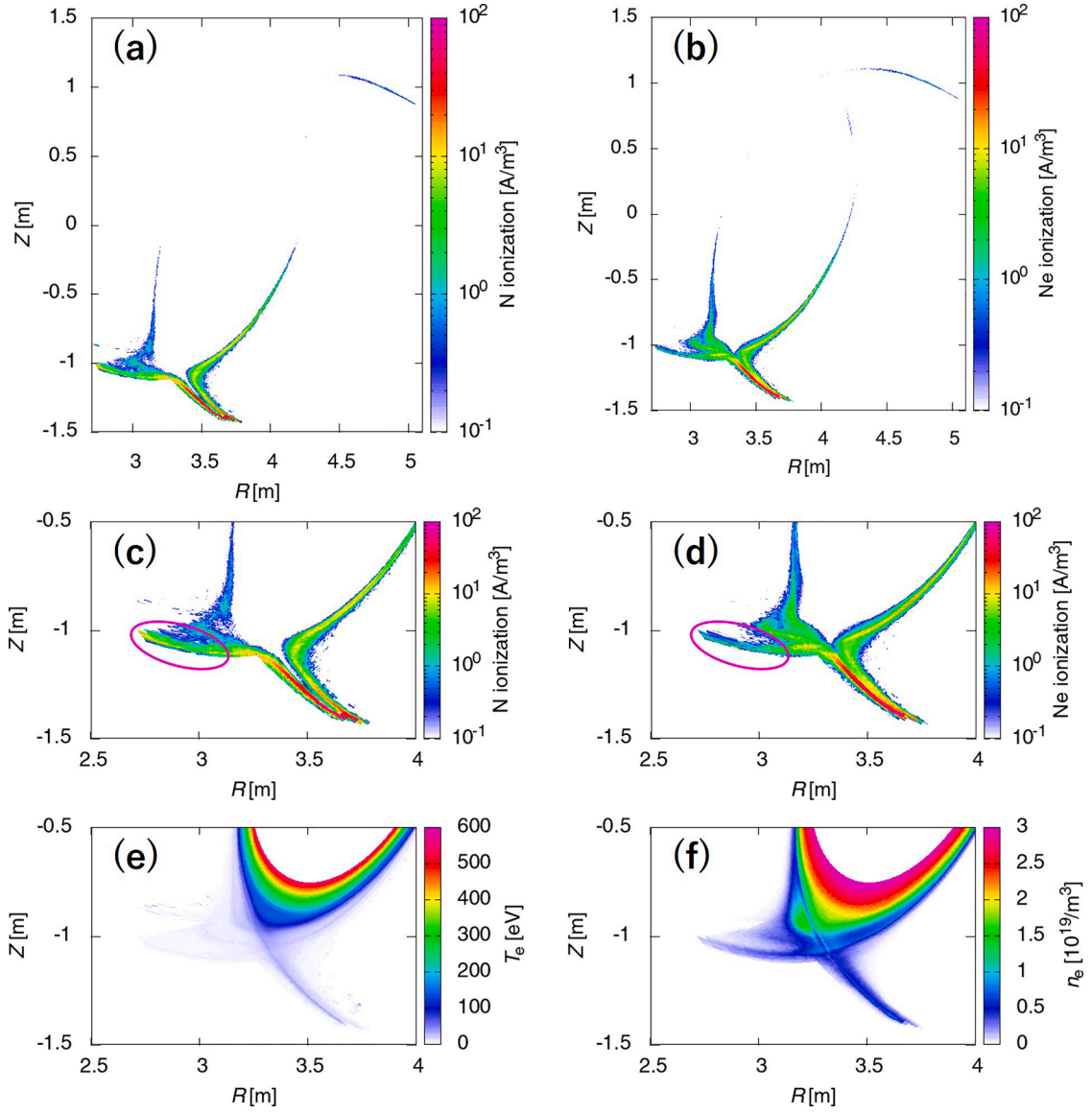

Fig. 8. Ionization rate profiles calculated by EMC3-EIRENE for (a) nitrogen, (b) neon atoms, and (c, d) their enlarged view at the poloidal cross section of the 5.5-L port. (e) electron temperature profile, and (f) electron density profile at the same cross section.

the lower-right leg was higher than the first ionization energy both of N and Ne, the lower T_e in the lower-left leg made the difference in the ionization enhancement in the lower-left leg between the N and Ne cases.

Fig. 9 (a) shows the magnetic field lines traced from the lower-left divertor leg in Fig. 8 (c) and (d). The lines shown in red from 5.5-L continued toward counterclockwise in toroidally and passed through the field of view of the IRVB. To compare the field lines and the extracted radiation structure in the second PC, two cross symbols are put in Fig. 6 (b) which are the local maximum of the second PC. The coordinates of the two points are $(R, \phi) = (3.564\ \text{m}, 202.2°)$ and $(3.716\ \text{m}, 198.3°)$. The definition of the coordinates is shown in Fig. 1. Fig. 9 (b) shows the top view of the traced magnetic field lines. Fig. 9 (c) - (f) shows the closeups of 4L, 7R, and 8R divertors and the field of view of IRVB shown in Fig. 9 (b), respectively. Here, the red and pink lines indicate the field lines which pass within 0.1 and 0.2 m in the R direction from these points, respectively. As shown in Fig. 9 (b) and (e), some of the red lines were terminated at the 8R divertor where $I_{sat,\ div}$ most decreased by the N_2 seeding shown in Fig. 3 (h). Moreover, as shown in Fig. 9 (b), (c), and (d), pink lines were terminated at the 4L and 7R divertor where the rest of $I_{sat,\ div}$ reduction occurred by the N_2 seeding. Therefore, the radiative cooling by the N_2 seeding occurred especially in the lower-left leg at the seeding port, was along the second PC, and was terminated at the divertor where the heat load decreased. The three-dimensionally localized structure could be extracted by the IRVB, PCA, and the comparison with magnetic field line structure.

In the case of N_2 seeding from 5.5-L port, the radiation was localized in the toroidal section #6 - #8. Therefore, in the case of 3.5-L and 9.5-L seeding, the radiation will expand in the toroidal section #4 - #6 and #10 - #2. This is the reason why the radiation feature was not observed in the N_2 seeding from 3.5-L and 9.5-L port in Fig. 7. In addition, the magnetic field line structure shrank toward the N_2 seeding port (right bottom direction in Fig. 9 (f)), however, the second PC did not have such a structure. Impurity transport analysis especially in the ergodic layer is required for further investigation.

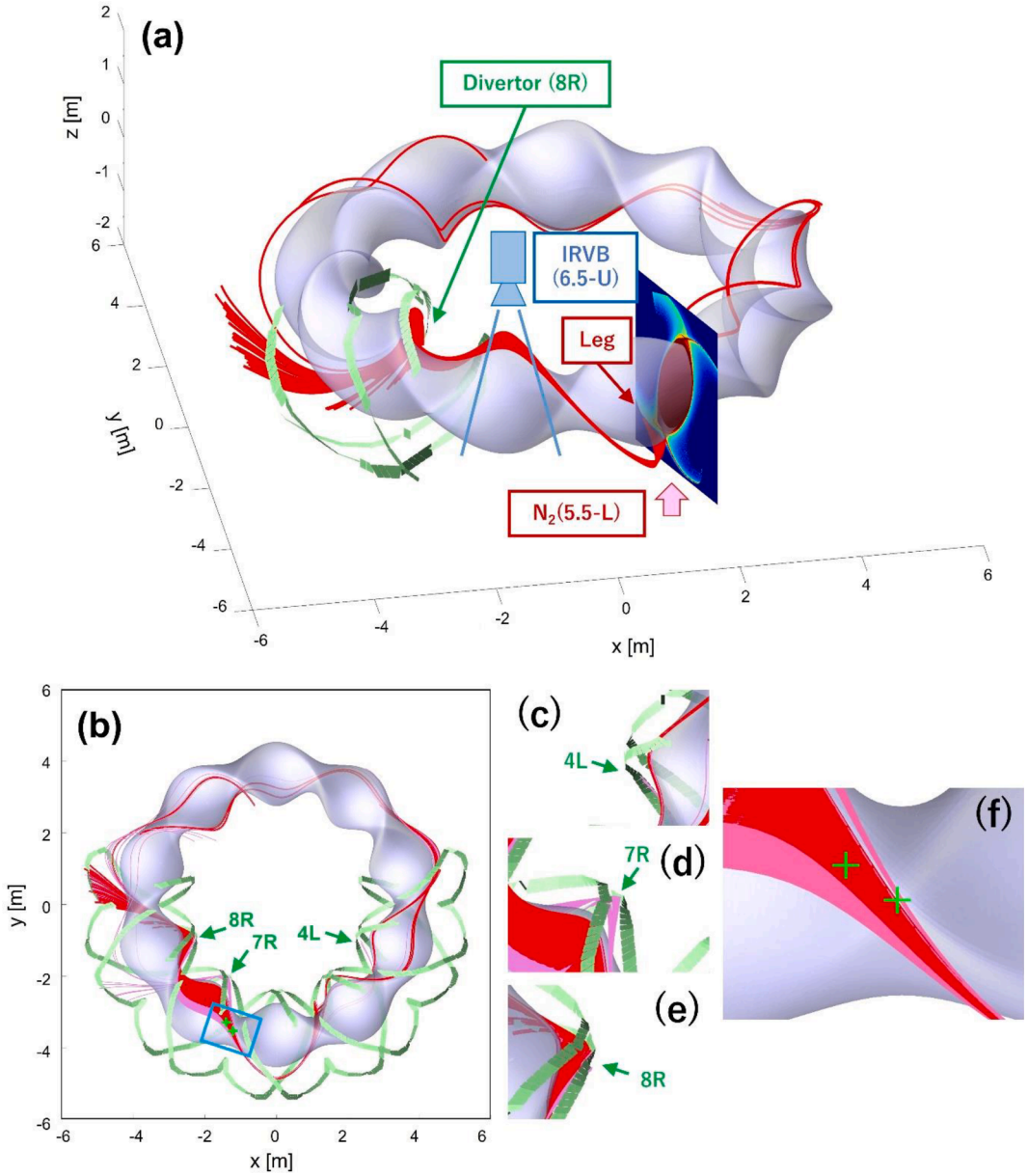

Fig. 9. Magnetic field lines traced from the divertor leg of the N_2 seeding port with the field of view of IRVB and divertor plates. (a) Bird view, (b) top view, and closeups of (c) 4L, (d) 7R, (e) 8R divertors, and (f) IRVB field of view. Cross symbols shown in (b) and (f) correspond to the symbols in Fig. 4 (b).

Summary

Three-dimensionally localization of radiative cooling due to N_2 seeding for divertor detachment was detected experimentally. The three-dimensionally localized structure was extracted using PCA from two-dimensional radiation images measured with an IRVB. PCA was applied to 34 images each in N_2 seeded plasmas with toroidally-asymmetric heat load reduction and in Ne seeded plasmas with toroidally-symmetric reduction. As the results, a radiation feature in N_2 seeded plasmas was found in one of the PCs. EMC3-EIRENE indicated that the ionization in one of the divertor legs is enhanced in nitrogen seeding compared with Ne seeding due to the difference in the first ionization energy. The magnetic field lines from the divertor leg were along the extracted radiation structure and were terminated by the divertor where the heat load decreased due to the N_2 seeding. These results can be concluded that three-dimensionally localized structure of radiative cooling was detected experimentally. The toroidal asymmetry of the divertor heat load reduction was also observed in the integration experiment of the detachment and the high-performance plasma in tokamaks such as EAST with ITER-like tungsten divertor. The advantage of the feature extraction using an IRVB and PCA is to detect the radiation localization without many diagnostics in toroidal direction. The technique can support to find the operation scenario using impurity seeding without toroidal asymmetry by detecting the radiation localization.

Data Availability Statement

The LHD data can be accessed from the LHD data repository at https://www-lhd.nifs.ac.jp/pub/Repository_en.html.

Declaration of Competing Interest

The authors declare the following financial interests/personal relationships which may be considered as potential competing interests: Kiyofumi Mukai reports financial support was provided by Japan Society for the Promotion of Science.

Data availability

Data will be made available on request.

Acknowledgments

The authors thank the LHD experiment group for their excellent support in the LHD experiments. This work was supported by JSPS KAKENHI Grant No. JP19K14689 and JP22K03583, by NIFS/NINS Grant No. NIFS18ULHH038.

References

[1] M.L. Reinke, J. Lore, J. Canik, B. LaBombard, D. Brunner, B. Lipschultz, R. Pitts, PSFC Research Report PSFC/RR-14-3, MIT, Cambridge, 2014.
[2] J.D. Lore, M.L. Reinke, B. LaBombard, B. Lipschultz, R.M. Churchill, R.A. Pitts, Y. Feng, J. Nucl. Mater. 463 (2015) 515–518.
[3] H. Tanaka, G. Kawamura, S. Masuzaki, M. Kobayashi, T. Akiyama, et al., Nucl. Mater. Energy 12 (2017) 241–246.
[4] B.J. Peterson, G. Kawamura, P.L. Giessen, K. Mukai, H. Tanaka, et al., Nucl. Mater. Energy 26 (2021), 100848.
[5] G. Kawamura, H. Tanaka, K. Mukai, B.J. Peterson, S.Y. Dai, et al., Plasma Phys. Control. Fusion 60 (2018), 084005.
[6] F. Effenberg, S. Brezinsek, Y. Feng, R. König, M. Krychowiak, et al., Nucl. Fusion 59 (2019), 106020.
[7] F. Reimold, M. Wischmeier, M. Bernert, S. Potzel, A. Kallenbach, et al., Nucl. Fusion 55 (2015), 033004.
[8] H.Q. Wang, L. Wang, S. Ding, A.M. Garofalo, X.Z. Gong, et al., Phys. Plasmas 28 (2021), 052507.
[9] C. Giroud, S. Brezinsek, R.A. Pitts, I.S. Carvalho, A. Huber *et al.*, High performance ITER-baseline discharges in deuterium with nitrogen and neon-seeding in the JET-ILW 28th IAEA Fusion Energy Conf. (Virtual), 2021. https://nucleus.iaea.org/sites/fusionportal/Shared%20Documents/FEC%202020/fec2020-synopsis/Synopsis0977.pdf.
[10] L.Y. Meng, L. Wang, H.Q. Wang, G.Z. Deng, H. Si, et al., Nucl. Fusion 62 (2022), 086027.
[11] B.J. Peterson, M. Osakabe, M. Shoji, N. Ashikawa, Rev. Sci. Instrum. 72 (2001) 923–926.
[12] K. Mukai, R. Abe, B.J. Peterson, S. Takayama, Rev. Sci. Instrum. 89 (2018) 10E114.
[13] R. Sano, B.J. Peterson, M. Teranishi, N. Iwama, M. Kobayashi, K. Mukai, S. N. Pandya, Rev. Sci. Instrum. 87 (2016), 053502.
[14] I.T. Jolliffe, Principal Component Analysis, Springer, New York, 2002.
[15] H. Abdi, L.J. Williams, Wiley Interdisciplinary Rev.: Comput. *Stat.* 2 (4) (2010) 433–459.
[16] Y. Feng, H. Frerichs, M. Kobayashi, D. Reiter, Plasma Phys. Control. Fusion 59 (2017), 034006.